FACTA UNIVERSITATIS
Series: **Mechanical Engineering** Vol. 5, N° 1, 2007, pp. 33 - 46

THE COMPARISON OF THEORETICAL AND EXPERIMENTAL RESULTS OF VELOCITY DISTRIBUTION ON BOUNDARY STREAMLINES OF SEPARATED FLOW AROUND A HYDROFOIL IN A STRAIGHT PLANE CASCADE

UDC 532.526 : 532.528

Božidar Bogdanović[1*], Jasmina Bogdanović-Jovanović[1], Živojin Stamenković[1], Pejo Majstorović[2]

[1]Faculty of Mechanical Engineering, A. Medvedeva 14, Nis, Serbia
[2]VP1094 Beograd
[*]E-mail: bozidar@masfak.ni.ac.yu

Abstract. *The demonstration of fluid flow through straight plane hydrofoil cascade, with separation of boundary layer from one side of a hydrofoil, was performed in water cavitation tunnel of the Military-Technical Institute in Zarkovo. Visualization of the flow was done by using an aniline color and air bubbles, and it was permanently recorded by a photo camera. Velocity field of the fluid flow around the hydrofoil was measured by the optical method using a Laser-Doppler Anemometry ID LDA.*
Using a photo of the flow pattern, it is easy to define boundary streamlines, which divide a zone of a primary ("uniform") flow from a vortex zone, in considerably separated boundary layer from a convex side of a hydrofoil, and a zone of a vortex shadding behind a hydrofoil. According to established boundary streamlines, velocity distribution on boundary streamlines was interpolated. Using a numerical program for solving Navier Stock's equations of turbulent flow, a flow was simulated in the same geometrical domain and for the same fluid flow as was used in the experiment. The results of this flow model were compared with experiment ones. According to the established boundary stream lines, using a model of potential fluid flow in the zone of main flow, velocity distribution on boundary streamlines was calculated theoretically. This velocity distribution was compared to the experimental results.

Key words: *Hydrofoil Cascade, Velocity, Boundary Layer, Vortex Shadding*

Received July 17, 2007

1. INTRODUCTION

A straight plane hydrofoil cascade consists of an infinite number of equal hydrofoils, equidistantly placed along a line, which is called the centerline of the cascade (y). The distance between compatible points of two neighboring hydrofoils is space between blades (t), while the geometric locus of center of circles inscribed in a hydrofoil defines the camber line of the hydrofoil.

Depending on whether the flow through the cascade is accelerated or decelerated, the cascades can be called accelerated (turbine) or decelerated (pump).

Experimental investigation of the flow through the straight plane cascade is performed in cascades made of the finite number of vanes, whose cross sections are hydrofoils equal to the hydrofoils of the discussed plane cascade. The number of the vanes cannot be less than five, and the examinational bench must be built to enable a plane flow through the hydrofoil cascade.

The flow visualization and the recording velocity field around a middle hydrofoil are conducted in the water cavitation tunnel of the Military-Technical Institute in Zarkovo. The tunnel has closed circulation of water, and Fig. 1 shows only an operating part of this tunnel, where a package of hydrofoils, packed between two Plexiglas panels, in the shape of straight plane cascade, is placed. Hydrofoils have an altitude of 100 mm. The sides of the operating part of the tunnel have Plexiglas windows.

In front of the operating part of the tunnel there is a collector placed (with longitude of 1245 mm) whose function is to create a uniform velocity field on the entry of the operating part of the tunnel. Contraction degree of the cross section of collector is 3,88, and at the entry of the collector there is honeycomb across the cross section.

Hydrofoils that form an experimental cascade are made on a programmed mill CNC using a contour milling on the defined surface. Hydrofoils are made of dural which has an aeronautical quality, and has an identification WH.3.1354. Plexiglas panels used in this case are of a high optical quality and they enable free pass of laser beam to the measuring points.

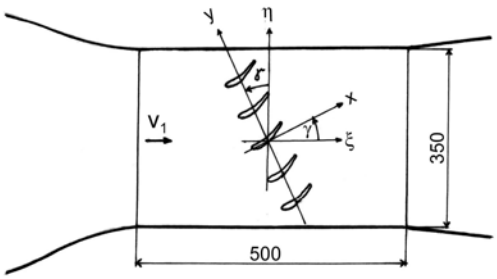

Fig. 1 Location of the hydrofoil in the operating part of the tunnel

2. RESULTS OF THE EXPERIMENTAL INVESTIGATION

Examined cascade is placed in such a way that the centerline of the cascade (y) forms an angle $\gamma=22^o$ with a vertical axis of the operating part of the tunnel (η), Fig. 1. In this position of the cascade, in flow velocity on the entry of the operating part of the tunnel $v_o=v_{\xi o}=5{,}32$ m/s, a flow separation on the whole convex side of the hydrofoil can be noticed.

Visualization of fluid flow is obtained by aniline color and air bubbles, and it was permanently recorded by a photo camera. In Fig. 2 gives a photo of fluid flow (for $v_o=v_{\xi o}=5{,}32$ m/s and $\gamma=22^o$).

In the experiment are measured horizontal (v_ξ) and vertical (v_η) components of flow velocities around the middle cascade hydrofoil, in the flow area limited by $\pm t/2$ from the middle hydrofoil. Velocities are measured by using a Laser-Doppler anemometry 1D LDA. Diameter of the focused laser beam is 0,88 mm. Measures are done in 247 chosen points of the flow area around the middle hydrofoil, and for each measurement point 800 signals are acquired. Results of measurements are given in Chart [1], and according to measured velocity and the photography of the flow (Fig. 2), the velocity distribution on boundary streamlines dividing the field of the main ("uniform") flow from the vortex field are produced by the flow separation from the convex side of the hydrofoil. The graph of velocity distribution is presented in Fig. 3, where the length coordinates are converted into a dimensionless form (according to hydrofoil chord length l=78,5 mm). Also velocity is converted to dimensionless form (according to velocity component normal to the centerline of the cascade, $v_{x1}=4{,}93$ m/s).

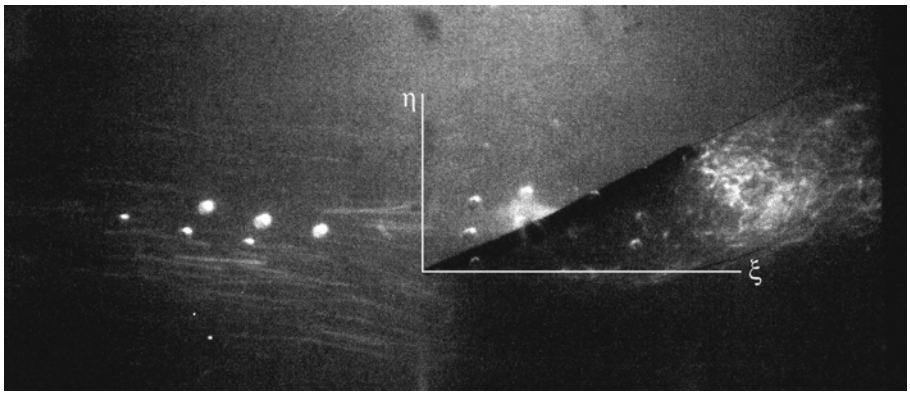

Fig. 2 Visualization of fluid flow- flow around the middle hydrofoil in the hydrofoil cascade

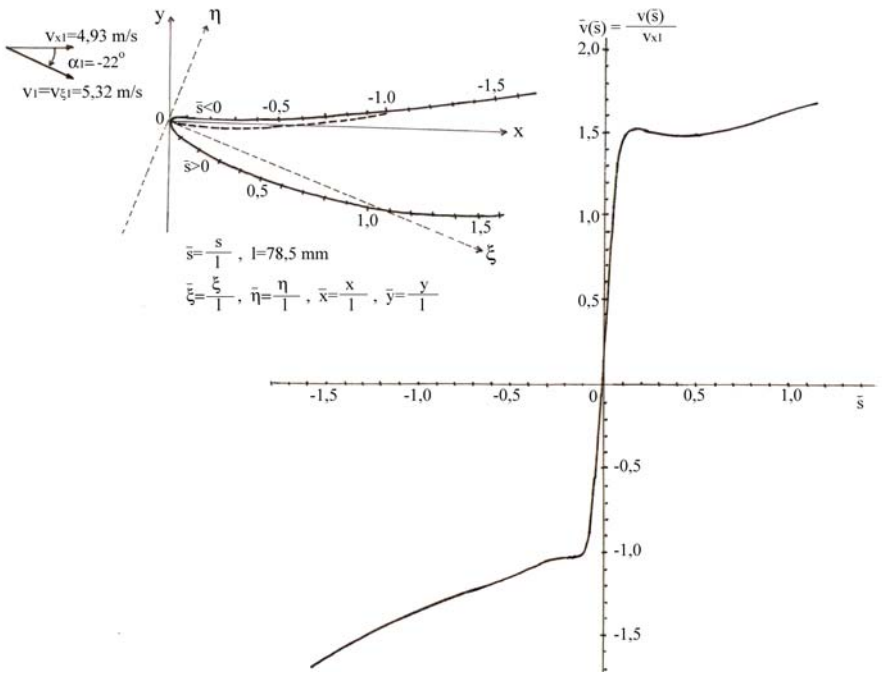

Fig. 3 Velocity distribution on boundary streamlines

Between measured velocity components v_ξ and v_η, in relation to horizontal (ξ) and vertical (η) axis of the tunnel and velocity components v_x and v_y, in relation to the centerline of cascade (y) and normal to centerline (x) (Fig. 1), there is relation:

$$v_x = v_\xi \cos\gamma + v_\eta \sin\gamma \,,\; v_y = -v_\xi \sin\gamma + v_\eta \cos\gamma \tag{1}$$

and an angle of the fluid flow, in relation to axis x, is calculated using a formula:

$$\alpha = \operatorname{arctg}(v_y / v_x) \,. \tag{2}$$

For $v_o=v_{\xi o}=5{,}32$ m/s ($v_\eta=0$) and $\gamma=22^o$, according to formulas (1) and (2), it is obtained that flow parameters faraway in front of the examined cascade are:

$$v_{x1}=4{,}933 \text{ m/s},\; v_{y1}=-1{,}993 \text{ m/s} \;(v_1=5{,}32 \text{ m/s}),\; \alpha_1=-22^o.$$

Connecting beginnings of both coordinate systems, Oξη and Oxy, for the leading edge of the middle hydrofoil, as is illustrated in Fig. 3, connection between coordinates ξ, η and x, y is described by equation:

$$x = \xi\cos\gamma + \eta\sin\gamma \,,\;\; y = -\xi\sin\gamma + \eta\cos\gamma \,. \tag{3}$$

3. CALCULATION OF THE FLOW THROUGH THE CASCADE USING A NUMERICAL SIMULATION

The set of equations which describe the processes of momentum, heat and mass transfer are known as the Navier-Stokes equations. These partial differential equations were derived in the early nineteenth century and have no known general analytical solution but can be discretized and solved numerically.

There is a number of different solution methods which are used in CFD codes. The most common, and the one that our software is based on, is known as the finite volume technique. In this technique, the region of interest is divided into small sub-regions, called control volumes. The equations are discretized and solved iteratively for each control volume. As a result, an approximation of the value of each variable at specific points throughout the domain can be obtained. In this way, one derives a full picture of the behavior of the flow.

3.1. CFD Methodology

CFD can be used to determine the performance of a component at the design stage, or it can be used to analyze difficulties with an existing component and it can lead to its improved design. The process of performing a single CFD simulation is split into four components:

1. ***Creating the Geometry/Mesh*** is the first pre-processing stage. The objective is to produce a mesh for input to the physics pre-processor. Before a mesh can be produced, a closed geometric solid is required. The geometry and mesh can be created in any software for geometry/mesh creation.

The basic steps involve:

1. Defining the geometry of the region of interest.
2. Creating regions of fluid flow, solid regions and surface boundary names.
3. Setting properties for the mesh.

2. ***Defining the Physics of the Model*** is the second pre-processing stage and it is used to create input required by the solver. The mesh files are loaded into the physics pre-processor. The physical models that are to be included in the simulation are selected. Fluid properties and boundary conditions are specified.

For solving the CFD problem the software which produces the required results in a non-interactive/batch process can be used. A CFD problem is solved as follows:

1. The partial differential equations are integrated over all control volumes in the region of interest. This is equivalent to applying a basic conservation law (for example, for mass or momentum) to each control volume.
2. These integral equations are converted to a system of algebraic equations by generating a set of approximations for the terms in the integral equations.
3. The algebraic equations are solved iteratively.

3. ***Solving the CFD Problem***. An iterative approach is required because of the non-linear nature of the equations, and as the solution approaches the exact solution, it is said to converge. For each iteration, an error, or residual, is reported as a measure of the overall conservation of the flow properties. How close the final solution is to the exact solution depends on a number of factors, including the size and shape of the control volumes

and the size of the final residuals. Complex physical processes, such as combustion and turbulence, are often modeled using empirical relationships. The approximations inherent in these models also contribute to differences between the CFD solution and the real flow. The solution process requires no user interaction and is, therefore, usually carried out as a batch process. The solver produces a results file which is then passed to the post-processor.

4. ***Visualizing the Results in the Post-processor.*** The post-processor is the component used to analyze, visualize and present the results interactively. Post-processing includes anything from obtaining point values to complex animated sequences.

Examples of some important features of post-processors are:

- Visualization of the geometry and control volumes
- Vector plots showing the direction and magnitude of the flow
- Visualization of the variation of scalar variables (such as temperature, pressure, etc.)
- Quantitative numerical calculations
- Animation
- Charts showing graphical plots of variables
- Hardcopy output.

3.2. Turbulence Models

The basic characteristic of turbulence is fluctuations of values in the flow field in time and space. It is a complex process, mainly because it is three dimensional, unsteady and consists of many scales. It can have a significant effect on the characteristics of the flow. Turbulence occurs when the inertia forces in the fluid become significant compared to viscous forces, and is characterized by a high Reynolds Number.

In principle, the Navier-Stokes equations describe both laminar and turbulent flows without the need for additional information. However, turbulent flows at realistic Reynolds numbers span a large range of turbulent length and time scales, and would generally involve length scales much smaller than the smallest finite volume mesh, which can be practically used in a numerical analysis. The Direct Numerical Simulation (DNS) of these flows would require computing power which is many orders of magnitude higher than available in the foreseeable future.

To enable the effects of turbulence to be predicted, a large amount of CFD research has concentrated on the methods which make use of turbulence models. Turbulence models have been specifically developed to account for the effects of turbulence without recourse to a prohibitively fine mesh and direct numerical simulation. Most turbulence models are statistical turbulence ones, as described below.

When looking at time scales much larger than the time scales of turbulent fluctuations, the turbulent flow could be said to exhibit average characteristics, with an additional time-varying, fluctuating component. For example, a velocity component may be divided into an average component, and a time varying component.

In general, the turbulence models are used to modify the original unsteady Navier-Stokes equations by the introduction of averaged and fluctuating quantities to produce the Reynolds Averaged Navier-Stokes (RANS) equations. These equations represent the mean flow quantities only, while modeling turbulence effects without a need for the reso-

lution of the turbulent fluctuations. All scales of the turbulence field are being modeled. Turbulence models based on the RANS equations are known as Statistical Turbulence Models due to the statistical averaging procedure employed to obtain the equations. Simulation of the RANS equations greatly reduces the computational effort compared to a Direct Numerical Simulation and is generally adopted for practical engineering calculations.

However, the averaging procedure introduces additional unknown terms containing products of the fluctuating quantities, which act like additional stresses in the fluid. These terms, called 'turbulent' or 'Reynolds' stresses, are difficult to determine directly and so become further unknowns.

The Reynolds (turbulent) stresses need to be modeled by additional equations of known quantities in order to achieve "closure." Closure implies that there is a sufficient number of equations for all the unknowns, including the Reynolds-Stress tensor resulting from the averaging procedure. The equations used to close the system define the type of turbulence model.

One proposal suggests that turbulence consists of small eddies which are continuously forming and dissipating, and in which the Reynolds stresses are assumed to be proportional to mean velocity gradients. This defines an 'eddy" viscosity model.

The eddy viscosity hypothesis assumes that the Reynolds stresses can be related to the mean velocity gradients and Eddy (turbulent) Viscosity by the gradient diffusion hypothesis, in a manner analogous to the relationship between the stress and strain tensors in laminar Newtonian flow. Here the Eddy Viscosity or Turbulent Viscosity has to be modeled.

Two equation turbulence models are very widely used, as they offer a good compromise between numerical effort and computational accuracy. Two-equation models are much more sophisticated than the zero equation models. Both the velocity and length scale are solved using separate transport equations (hence the term 'two-equation'). The k-ε and k-ω two-equation models use the gradient diffusion hypothesis to relate the Reynolds stresses to the mean velocity gradients and the turbulent viscosity. The turbulent viscosity is modeled as the product of a turbulent velocity and turbulent length scale. In two-equation models, the turbulence velocity scale is computed from the turbulent kinetic energy, which is provided from the solution of its transport equation. The turbulent length scale is estimated from two properties of the turbulence field, usually the turbulent kinetic energy and its dissipation rate. The dissipation rate of the turbulent kinetic energy is provided from the solution of its transport equation.

In the k-ε model the values of k and ε come directly from the differential transport equations for the turbulence kinetic energy and turbulence dissipation rate:

$$\frac{\partial(\rho k)}{\partial t}+\nabla\cdot(\rho U k)=\nabla\cdot\left[\left(\mu+\frac{\mu_t}{\sigma_k}\right)\nabla k\right]+P_k-\rho\varepsilon \tag{4}$$

$$\frac{\partial(\rho \varepsilon)}{\partial t}+\nabla\cdot(\rho U \varepsilon)=\nabla\cdot\left[\left(\mu+\frac{\mu_t}{\sigma_\varepsilon}\right)\nabla \varepsilon\right]+\frac{\varepsilon}{k}(C_{\varepsilon 1}P_k-C_{\varepsilon 2}\rho\varepsilon)\,, \tag{5}$$

where P_k is the turbulence production due to viscous and buoyancy forces, which is modeled using:

$$P_k = \mu_t \nabla U \cdot (\nabla U + \nabla U^T) - \frac{2}{3}\nabla \cdot U(3\mu_t \nabla \cdot U + \rho k) + P_{kb} \,. \tag{6}$$

In this model is assumed that turbulence viscosity μ_t is linked to turbulence kinetic energy k and dissipation ε via relation: $\mu_t = c_\mu \rho k^2 / \varepsilon$, where c_μ is a constant. Values of constants are: $C_{\varepsilon 1} = 1{,}44$, $C_{\varepsilon 2} = 1{,}92$, $\sigma_k = 1$, $\sigma_\varepsilon = 1{,}3$, $c_\mu = 0{,}09$.

3.3. Numerical Simulation

According to the CFD methodology, an exact geometrical model and the mesh are created. The fluid domain consists of two subdomains (collector and chamber with a cascade of three hydrofoils). The mesh is irregular and it contains 546247 nodes and 1867089 elements (tetrahedral and prismatic). All the initial parameters, such as flow rate and initial pressure are set. The k-ε turbulent model is used.

The solution, for the required convergence criteria (RMS normalized values of the equation residual is 10^{-5}), is achieved in 457 iterations.

The final step is an analysis of the results of the numerical simulation and their comparison to the experimental ones. Fig. 4 presents the boundary streamlines obtained by numerical simulation, as well as by the experimental measurements. This analysis shows a good agreement between the numerical results and the experimental measurements.

Velocity distribution is shown in Fig. 5 where the same trend line of the compared velocities on the boundary streamline can be clearly noticed. Velocity magnitudes obtained by the experiment are higher than velocities obtained by numerical simulation. The reasons for this inequality can be found in friction losses that are not counted. Also, there is a great velocity changing in the surrounding of the boundary streamline, due to high vorticity in that particular area.

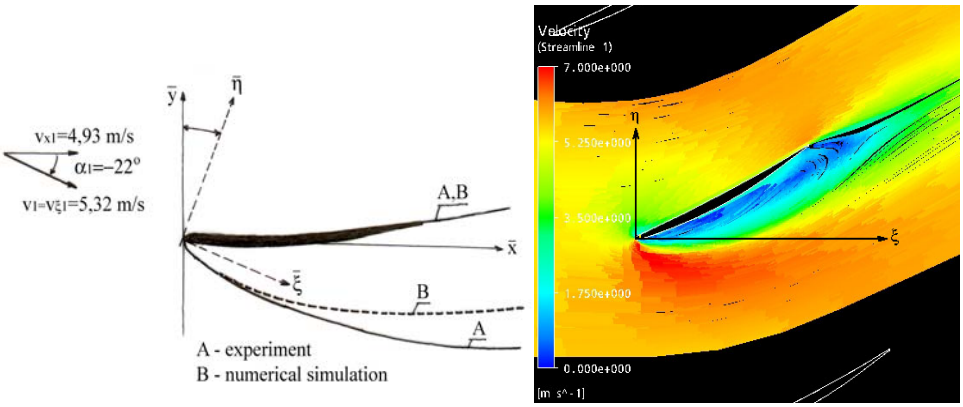

Fig. 4 Boundary streamlines: a) comparison with experimental results, b) numerically obtained boundary streamlines

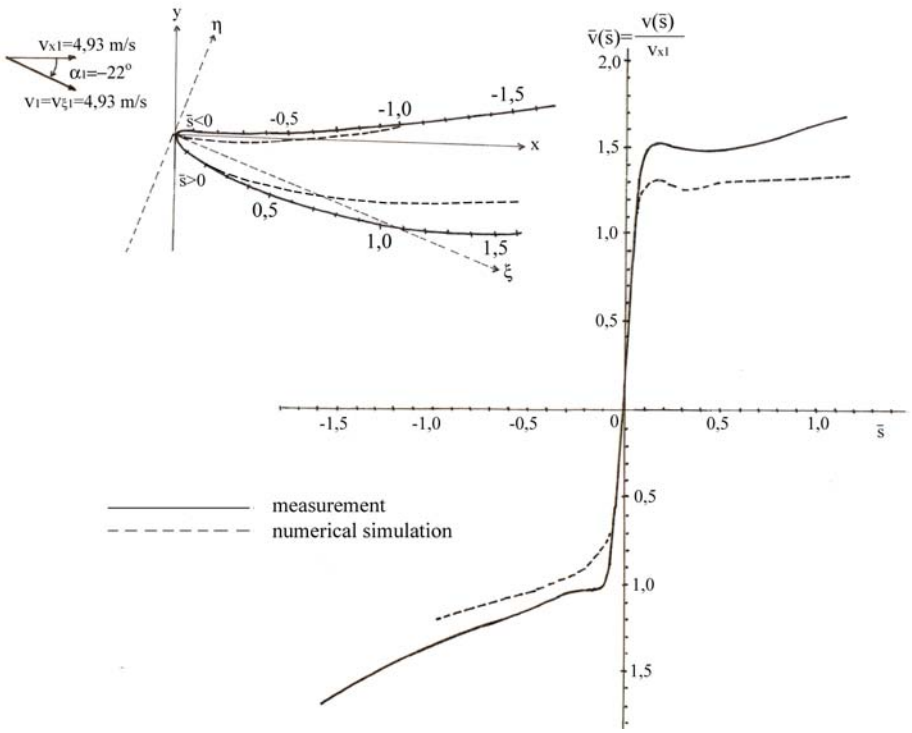

Fig. 5 Comparison of functional graph $\bar{v}(s) = v(s)/v_{1x}$ obtained by experimental measurements and numerical simulation

4. Calculation of the Flow Through the Cascade of Semihydrofoils Using a Conformal Mapping on the Flow in the Belt

Extending hydrofoils of the straight plane cascade with contour of the vortex shadding behind hydrofoil, as is shown in Fig. 6, a cascade of semihydrofoils is obtained.

The flow through the semihydrofoil cascade, in the area between two streamlines, on the distance which is equal to the space between blades (t), can be mapped to the flow in the indefinite belt $-\pi/2 \le I_m\zeta \le \pi/2$, with singular point $\zeta=0$, an area in front of the semihydrofoil cascade is mapped indefinitely. In $\xi=0$ is source with fluid discharge $Q=v_{x1}\cdot t=v_1\cos\alpha_1\cdot t$ and free vortex with circulation $\Gamma_1= v_{y1}\cdot t=v_1\sin\alpha_1\cdot t$.

The longitudinal coordinates of the hydrofoil sides left of stagnation point s=0, are formally given a negative sign ($s_b=s<0$). Flow velocities along this hydrofoil side are formally also with a negative sign ($s<0$, $v(s)<0$).

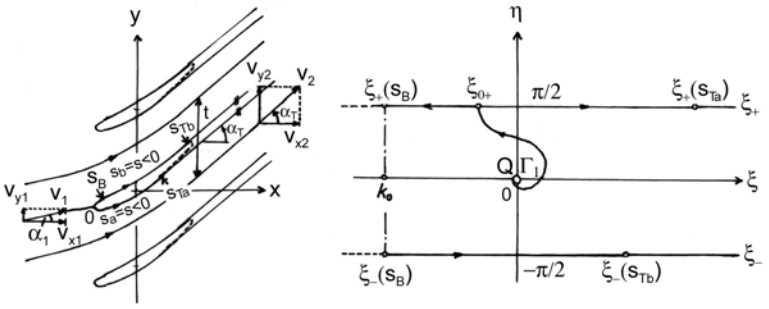

Fig. 6 Conformal mapping method for hydrofoils of the straight plane cascade

For simplicity, character ξ_+ is used for $\zeta=\xi+i\pi/2$ and character ξ_- for $\zeta=\xi-i\pi/2$. Hydrofoil contour is mapped to the contour of the belt (ξ_+ and ξ_-).

General values of velocity potential for contour of the belt (taking values of the function arcctgsh$\xi_\pm$ in interval from 0 to π) are:

$$\Phi(\xi_\pm)=\frac{Q}{2\pi}[\ln \mathrm{sh}\xi_\pm+\xi_\pm \pm \mathrm{tg}\alpha_1\cdot \mathrm{arcctgsh}\xi_\pm],$$

and concerning that it has many values:

$$\Phi_n(\xi_\pm)=\Phi(\xi_\pm)\pm n\frac{Q}{2}\mathrm{tg}\alpha_1=\Phi(\xi_\pm)\pm\frac{\Gamma_1}{2}n, \qquad n=0,\pm1,\ldots$$

Velocity distribution around the contour belt is defined by function:

$$V(\xi_\pm)=\frac{Q}{2\pi}\left[1+\mathrm{th}\xi_\pm\pm\frac{\mathrm{tg}\alpha_1}{\mathrm{ch}\xi_\pm}\right],$$

and the stagnation point is: $\xi_{01}=\xi_{01\pm}=(\xi_{01+}$ ili $\xi_{01-})=\ln(\pm\mathrm{tg}\alpha_1)$.

For $\alpha_1>0$, the stagnation point on the leading edge of the semihydrofoil (s=0) is mapped to stagnation point ξ_{0+} on ξ_+ contour belt, as is shown in Fig. 6b. Hydrofoil side $s_a=s>0$ is mapped to $\xi_+>\xi_{0+}$, and side $s_b=s<0$ (Fig. 6a) is mapped with its smaller part to $\xi_+<\xi_{0+}$, and with its larger part to ξ_- contour belt. According to the character of the velocity potential function of contour belt ($\Phi_n(\xi_\pm)$), it is proved [2] that on $\xi_\pm \le -k_0$ ($k_o = 5 \div 10$), with indefinite extension, one and the same point of s_b semihydrofoil side (point S_B in Fig. 6a) is mapped.

For $\alpha_1=0$, the stagnation point on the leading edge of semihydrofoil (s=0) is mapped, with indefinite extension, to $\xi_\pm \le -k_0$. On $\xi_+ > -k_0$ is mapped semihydrofoil side $s_a=s>0$, and semihydrofoil side $s_b=s<0$ is mapped to $\xi_- > -k_0$.

For $\alpha_1<0$, the stagnation point on the leading edge of the semihydrofoil is mapped to stagnation point ξ_{0-} on ξ_- contour belt. Semihydrofoil side $s_b=s<0$ is mapped to $\xi_->\xi_{0-}$, and semihydrofoil side $s_a=s>0$ is mapped with its smaller part to ξ_- contour belt, and with its larger part to ξ_+ contour belt. On $\xi_\pm \le -k_0$ is mapped, with indefinite extension, one and the same point of s_a semihydrofoil side.

Considering mapping character of the semihydrofoil contour to the contour belt, it is done a program (in Fortran) for calculation of dimensionless velocity distribution around hydrofoil contour ($\bar{v}(s) = v(s)/v_{1x}$) and angle of attack (α_1), for an accepted stagnation point on the leading edge of the hydrofoil [2]. All longitudinal parameters of the cascade, in this program [2, 3], are derived to the dimensionless form, considering that a chord is equal to unity (l=1). Reading parameters of the program are: α_{1p}- inlet angle of camber line, $\bar{t}$ - relative space between blades, l_s – camber line of the hydrofoil, α_T - angle of lengthening hydrofoil to the semihydrofoil, s_{Ta} – last calculating point on the hydrofoil side s>0 and s_{Tb} – last calculating point on the hydrofoil side s<0, as it is a subprogram FUNCTION ALFA(S), which defines a function $\alpha(s)$, where α - tangent angle of the semihydrofoil contour, measured related to the x-axis of the cascade. Iterative procedure of calculation is done when the difference between obtained angle α_1 and this angle obtained in previous iterative step is less than $0{,}1^o$. At the end of iterative procedure, velocities $\bar{v}(s) = v(s)/v_{1x}$ with step $\Delta s=0{,}01$, are printed, and are also printed correspondence of mapped points $s(\xi_+)$ and $s(\xi_-)$ and longitudinal coordinate of the point on the hydrofoil contour, which is mapped, with indefinitely extension, on $\xi_\pm \le -k_0$ (point S_B, Fig. 6).

Knowing the velocity distribution on hydrofoil contour $\bar{v}(s) = v(s)/v_{1x}$ for angle of attack α_1, for any other angle of attack α_1^*, the velocity distribution can be calculated by using an equation:

$$\frac{v^*(s)}{v^*_{x1}} = \frac{1 + th\xi_\pm(s) \mp \dfrac{tg\alpha_1^*}{ch\xi_\pm(s)}}{1 + th\xi_\pm(s) \mp \dfrac{tg\alpha_1}{ch\xi_\pm(s)}} \frac{v(s)}{v_{x1}} \tag{7}$$

The previously mentioned program for calculating a fluid flow through the semihydrofoil cascade is designed for the flow with shockless attack to the cascades with larger density, when the hydrofoils are extended with a thin vortex shadding, as is shown in Fig. 6a. The validity of results obtained by this calculation is confirmed in numbering experimental research projects that are conducted for straight hydrofoil cascades with shockless attack to the hydrofoil cascade (where the stagnation point is in the leading edge).

It is interesting to compare the results of calculation obtained by the program to the experimental ones for the case when fluid flow is completely separated of the one side of the hydrofoil, as is shown in Fig. 2. According to the picture of the fluid flow through the hydrofoil cascade (Fig. 2), for $\alpha_1=-22^o$, pressure sides of hydrofoils are extended with suitable contour of the vortex shadding, and suction sides of hydrofoils are changed with contour of the stream lines which limit an area of vortex flow separation (on the convex side of the hydrofoils).

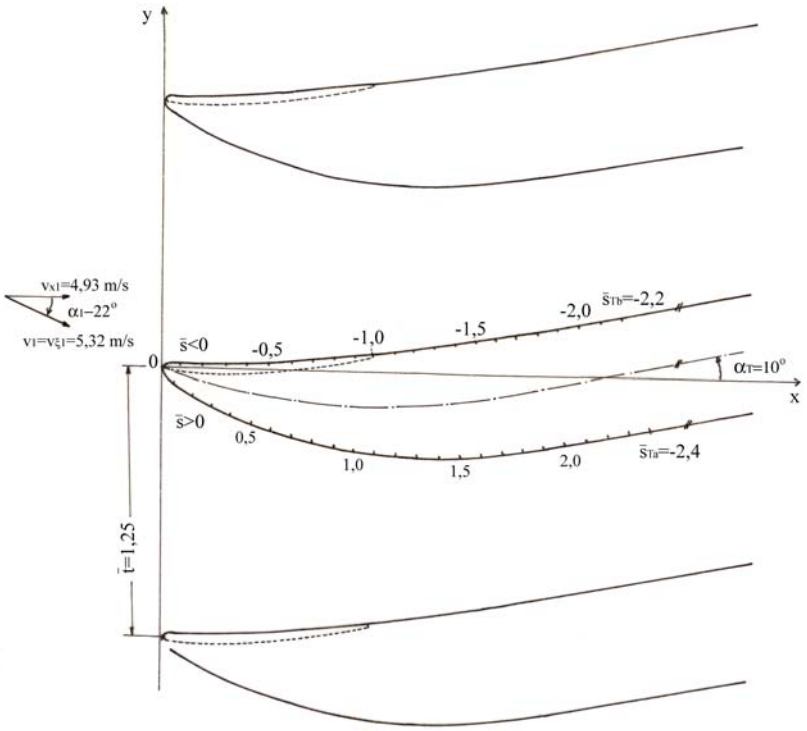

Fig. 7 Semihydrofoil cascade

The semihydrofoil cascade, obtained accordingly, is shown in Fig. 7. Since all the longitudinal parameters, in the program, are derived to the dimensionless form, according to unity chord of extended hydrofoils (l=1), in Fig. 7, a chord of a fictive hydrofoil is defined, which, by extension with line edged at $\alpha_T=10^o$, becomes the semihydrofoil.

Between dimensionless coordinates ($\bar{x}$, $\bar{y}$, $\bar{s}$, $\bar{l}$) in Fig. 7 and real coordinates (x, y, s, l) of the examinational bench, there is a connection:

$$x[mm] = 174{,}8 \cdot \bar{x}, \quad y[mm]=174{,}8 \cdot \bar{y}, \ldots$$

According to the results of the calculation velocity distribution along a semihydrofoil contour, Fig. 8 gives a functional graph $\bar{v}(s) = v(s)/v_{1x}$ (full line), and a graph of this function obtained by experimental measurements on the examinational bench is illustrated using a dashed line.

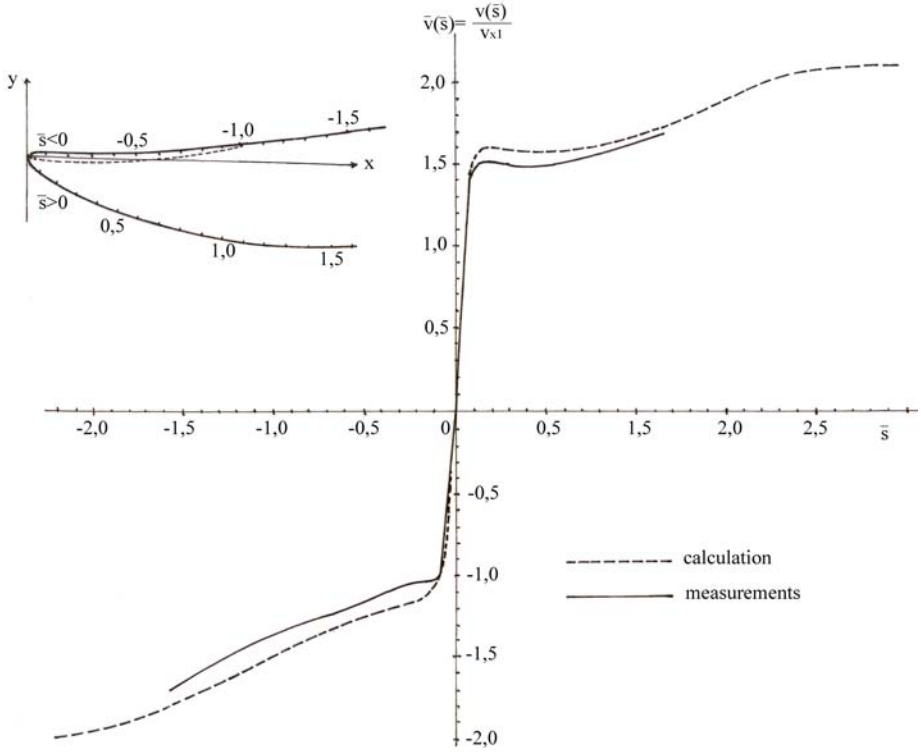

Fig. 8 Comparison of functional graph $\overline{v}(s) = v(s) / v_{1x}$ obtained by calculations and experimental measurements

The measured velocities, unfortunately, do not cover the whole field of calculated velocities, but, in spite of this, it can be concluded that the presented method can be used, relatively well, in cases of flow with extreme separation of the boundary layer from one side of a hydrofoil. Slightly larger velocity values, obtained by calculation, are result of neglected fluid flow through a vortex shadding zone.

CONCLUSION

The theoretical results follow the experimental ones with satisfying accuracy, especially the character of the graph modification. Velocity distribution on boundary streamline, in the case of numerical simulation, is little lower comparing to the experimental one, due to the different boundary streamline, which is in the numerical simulation closer to the convex side of the hydrofoil.

The results obtained by numerical simulation according to the model of potential flow are little higher comparing to the experimental results, which is surprising at the first glance, because the flow in the domain has a significant flow separation from the one side of the hydrofoil. The experimental results are between the numerical results obtained us-

ing Navier-Stocks equations for turbulent flow and those obtained using the model of potential flow in the area of the main ("uniform") flow.

REFERENCES

1. Bogdanović Božidar, "Apendix to determination of flow through cascade of axial turbomashinery", doctoral thesis, Faculty of Mechanical Engineering in Nis, 1982.
2. Bogdanović Božidar, "Calculation of potential flow through straight plane hydrofoil cascades using a method of conformal mapping", monograph, Faculty of Mechanical Engineering in Nis, 1999.
3. Bogdanović B., Milanović S.: " Solution of the direct problem in theory of flow through straight plane profile cascade by using coformal mapping into band $-\pi/2 \le \mathrm{Im} Z \le \pi/2$ ", Fakta universitatis, Series mechanical enginering, (str. 809 ÷ 816), Vol. 1, N^o 7, 2000.
4. Majstorović Pejo, "Application of Laser-Doppler method for indirect measurment of flow values of thes-traight plane hydrofoil cascade", master thesis, Faculty of Mechanical Engineering in Nis, 2005.
5. Ristić, S., Vitić, A., Grozdanovski, D. Baždarenje vodenokavitacionog tunela i merenje raspodele brzine strujanja po tetivi krila pomoću LDA, Vazduhoplovstvo, 1993., 9-10, Beograd.
6. Ristić, S., Vitić, A., Analysis of the Accuracy of the Third Component of Flow Velocity Measurements for a 3-component, 3-color Laser Doppler Anemometer. 21. Congress of the ICAS , 1998, 13 - 18 sept. Melbourne, Australia.
7. Saša Milanović, "Calculation of the spatial fluid flow through axial turbomashinery as a complex of two two-simensional fluid flows ", master thesis, Faculty of Mechanical Engineering in Nis, 1996.
8. Watrasiewich, B. M., Rudd, J. J. Laser Doppler Measurements. London - Boston, Butterworths, 1976.
9. Wilcox,D.C., "Turbulence modeling for CFD", DCW Industries, 2000, p.314.

UPOREĐIVANJE RASPOREDA BRZINA NA GRANIČNIM STRUJNICAMA ODLEPLJENOG STRUJANJA OKO PROFILA PRAVE RAVANSKE REŠETKE

Božidar Bogdanović, Jasmina Bogdanović-Jovanović, Živojin Stamenković, Pejo Majstorović

Demonstracija strujanja kroz pravu ravansku profilnu rešetku, sa izrazito odlepljenim graničnim slojem od jedne strane profila, izvršena je u vodeno-kavitacionom tunelu (VKT) Vojno-tehničkog instituta u Žarkovu. Vizualizacija strujanja izvršena je pomoću anilinskih boja i vazdušnih mehurića, a trajno je registrovana fotografisanjem. Brzinsko polje strujanja oko profila mereno je optičkom metodom pomoću Laser Dopler anemometarskog sistema 1D LDA. Korišćenjem fotografije strujne slike, lako se geometrijski definišu granične strujnice, koje razdvajaju zonu osnovnog ("uniformnog") strujanja od zone vrtloga u izrazito odlepljenom graničnom sloju od leđne strane profila i zone vrtložnog traga iza profila.Prema izmerenim brzinamau strujnom prostoru oko profila interpoliran je grafik rasporeda brzina po ovim graničnim strujnicama. Korišćenjem programa za numeričko rešavanje Navije-Stoksivuh jednačina za turbulentno strujanje, teorijski je simulirano strujanje u geometrijski istom prostoru i za istu brzinu dotoka struje rešetki, kao i kod eksperimenta. Rezultati ovako modeliranog strujanja upoređena su sa eksperimentalnim rezultatima. Na osnovu ovako utvrđenih graničnih strujnica, korišćenjem modela potencijalnog strujanja u zoni osnovnog strujanja, teorijski je određen raspored brzina duž ovih graničnih strujnica. Ovaj raspored brzina upoređen je sa eksperimenalno dobijenim rasporedom brzina.

Ključne reči: *rešetka profila, brzine, granični sloj, vrtložni trag*